THE JOURNAL OF PHYSICAL CHEMISTRY A

Article

Cite This: J. Phys. Chem. A 2018, 122, 7540−7547

pubs.acs.org/JPCA

Activation of Reactions in the Complex Region Using Microwave Irradiation

Dandan Ma,[†,#] Xuefen Tian,[†,#] Lifen Guo,[†] Jie Mou,[†] Sen Lin,[*,‡] and Jianyi Ma[*,†]

[†]Institute of Atomic and Molecular Physics, Sichuan University, Chengdu, Sichuan 610065, China

[‡]State Key Laboratory of Photocatalysis on Energy and Environment, College of Chemistry, Fuzhou University, Fuzhou 350002, People's Republic of China

ABSTRACT: Many mode-specific behaviors in the gas phase and at the gas-surface interface have been reported in the past decades. Infrared activation of a reagent vibrational mode is often used to study these reactions. In this work, an inexpensive and easily applied scheme using microwave irradiation is proposed for activating complex-forming reactions by transferring populations between closely spaced resonances. The important combustion reaction of H + O_2 ↔ O + OH is used as a model system to demonstrate the feasibility of the proposed approach. The existence of a nonzero transition dipole moment matrix element between two highly excited resonance states separated by a small energy gap in the model system may allow one to use microwave irradiation to intervene and control the model reaction. The high energy resonance states of the model reaction can also release their energy by photon emission, which is in agreement with the experimentally observed chemiluminescence process.

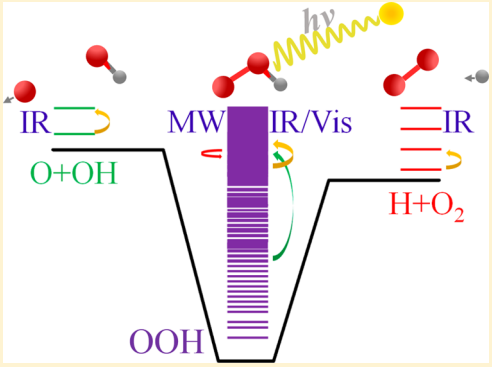

INTRODUCTION

Mode specificity and nonstatistical behavior are of great importance for many reactions.[1−4] Mode specificity means that the reactivity is not the same for different mode excitations, even when the total energies of the system are the same. The reactivity can be described by the rate constant, reaction yield, reaction branch ratio, and other quantities. This phenomenon has been observed in the gas phase and in surface processes. A unimolecular process shows sometimes nonstatistical behaviors.[1,5] For example, on the time scale of the reaction, the intramolecular vibrational relaxation (IVR) may not be complete even at an internal energy that is much higher than the dissociation threshold. Only few of the vibrational modes may be active for some multiatom systems. For bimolecular reactions involving an atom and a diatomic molecule, Polanyi's rules suggest that vibrational excitation of the reagent is an efficient means to enhance reactivity if the barrier is in the product channel.[6,7] Recently, the sudden vector projection (SVP) model has been advanced[8] to explain experimentally observed mode specificity behaviors for bimolecular reactions involving polyatomic reactants.[3,9]

Because of the nonstatistical features of many chemical reactions, the effectiveness of reactivity promotion is generally not expected to be the same for all internal modes and translational degrees of freedom. It is thus possible to use mode specificity to control reactions by changing the distribution of the rovibrational states of the corresponding molecules. Recently, infrared activation of a reactant vibrational mode has been a common technique to study mode-specific reactions in the laboratory.[4,10−12] Unfortunately, high-intensity IR laser sources are relatively expensive, and the required IR frequency strongly depends on the reaction system according to the characteristics of the mode-specific reactions. It is therefore vital to examine whether there exists an alternative approach that avoids the use of an IR laser and enables efficient and convenient promotion of the reaction by taking advantage of mode specificity behaviors.

In many chemical reactions, one or more strongly interacting regions (reaction intermediates) is located between the reactants and products. The densities of the rovibrational states in these regions are usually much higher. Similarly, the anharmonicity and coupling among the different vibrational modes are also very significant in the interaction regions. The high state density and anharmonicity mean that the vibrational behavior changes significantly even with small changes in the energy of the system. For a hypothetical example, for the three vibrational modes of a triatomic molecule, denoted as 1, 2, and 3, the $1^5 2^6 3^1$ and $1^0 2^5 3^{12}$ high energy states of this molecule may have similar energies but very different vibrational levels, and the anharmonicity of this molecule makes the $\langle 1^5 2^6 3^1 | \bar{u} | 1^0 2^5 3^{12} \rangle$ transition dipole moment not equal to zero. Therefore, it is possible to promote the transition between two such states using low-energy and high-intensity photons, such as microwave radiation, which changes the energy level distribution of the reaction intermediate. When these states

Received: July 5, 2018
Revised: August 23, 2018
Published: August 30, 2018

DOI: 10.1021/acs.jpca.8b06442
J. Phys. Chem. A 2018, 122, 7540−7547

have different vibrational properties, this scheme could be used to promote a reaction.

Actually, since 1986, microwave-assisted synthesis in household microwave ovens has become a popular, unconventional technique in organic chemistry in addition to conventional heating methods.[13−15] Microwave-assisted reactions are characterized by several features that cannot be reproduced by conventional heating.[16,17] In this work, we investigate the possibility of activation of the chemical reaction in the interaction region using microwave irradiation. The H + O_2 ↔ O + OH reaction is used as a model reaction to illustrate how microwave irradiation affects the distribution of the vibrational states of the HO_2 complex.

As shown in Figure 1, the energy scheme indicates that the model reaction occurs adiabatically at a ground state potential

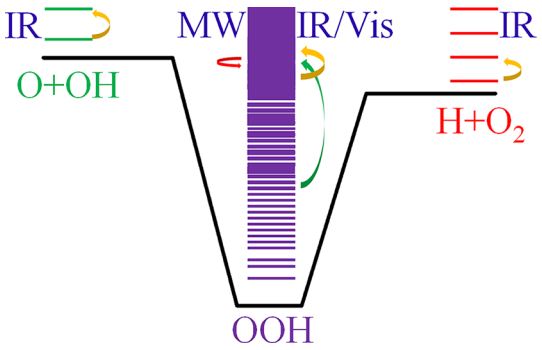

Figure 1. Scheme of microwave-involved mode-specific dynamics for H + O_2 ↔ O + OH reactions. In the reactant and product region, only infrared light is useful for adjusting the corresponding vibrational states. In the complex region, infrared light, visible light and microwave light can be used to affect the vibrational states.

energy surface characterized by a deep well (2.4 eV relative to the H + O_2 asymptote) and large exothermicity.[18] The presence of two oxygen atoms results in a high vibrational state density for the HO_2 intermediate in the high energy region. Additionally, the reported experimental rovibrational spectrum contains abundant structures of the vibrational and rotational excitations.[19−21] Therefore, we believe these features of the HO_2 system make it highly suitable for the investigation of microwave-involved dynamics processes. For H + O_2 ↔ O + OH reactions and other complex-forming reactions, the number and density of the vibrational states in the complex region are much larger than those in the reactant or product regions. This means that the reaction complex region provides more possibilities for controlling the reactions by using different frequencies of light, especially by microwave irradiation. The population of the resonance states of the reaction complex will be changed by the absorption or emission of the photons, leading to the changes in the reaction probability and the distribution of the rovibrational states of the product. The probability distribution of the internal states must depend on the frequency and the intensity of the external photon field. In other words, we can control molecular reactions by adding a frequency- and intensity-dependent external photon field. Unfortunately, due to the abundance of the internal states involved in the molecular reaction under an external photon field, statistical behavior will play an important role, and it is difficult to control a particular vibrational state using this approach.

The control of mode-specific reactions in the interaction region has an additional benefit in that the reaction complex has six additional degrees of freedom (DOF) for the internal vibration compared to that of the reactants for bimolecular reactions in general, and the presence of additional degrees of freedom means that more reaction channels may be activated by the external photon field. (For a bimolecular reactions involving molecule with M atom and molecule with N atom, the total controllable vibrational DOF is 3(M + N) − 12 in the reactant region, however, the value is 3(M + N) − 6 for the reaction complex in the interaction region.) Even for the H + CN ↔ HCN triatomic reaction, which includes an HNC ↔ HCN isomerization process, it is clear that the bending excitation of the HNC angle will promote isomerization, whereas the bending mode does not exist in the H + CN reactants.

Whether microwave irradiation can be used to effectively control reactions depends on two factors. (1) The transition dipole moment between the adjacent quantum states within the range of microwave energy must be large enough. (2) The vibrational mode of the transition must allow adjacent states to change obviously. These two factors must be system dependent. In general, a system that has more atoms and larger polarity is more likely to meet these two conditions. Without the loss of generality, the H + O_2 ↔ O + OH triatomic reaction is used to check these two conditions numerically.

METHODS

In this work, we use the version of the Xu−Xie−Zhang−Lin−Guo (XXZLG) potential energy surface (PES) for the HO_2 system[18] to obtain high excited vibrational wave functions. Density functional theory (DFT) and the neural network (NN)[22−25] method are used to construct the dipole moment surface (DMS). The Lanczos algorithm[26−28] is used to generate the wave functions and the transition dipole moments for the high excited vibrational states. In detail, for the potential energy surface of the electronic ground state of the HO_2 system, we use the XXZLG PES[18] obtained using the Davidson-corrected internally contracted multireference configuration interaction (icMRCI+Q) method with the AVQZ basis set. The dipole moment is calculated by DFT with the M06 functional[29] and PVTZ basis set using the Gaussian 09 program.[30] The DMS is fitted by an NN method using the input layer of Jacobi coordinates of the HO_2 system.[24,31] The explicit form of the base functions in the neurons can be readily found.[25,31] We choose to use two hidden layers with 15 and 20 neurons, respectively. In each NN fitting, the data are divided randomly into three sets, namely, the training (90% of the data points), validation (5%), and test (5%) sets. All NN fittings are performed using the Levenberg−Marquardt algorithm.[32]

The bound vibrational states up to the reactive region of HO_2 are calculated by solving the bound state Schrödinger equation with the total angular momentum $J = 0$. The corresponding Hamiltonian in the Jacobi coordinates can be expressed as

$$\hat{H} = -\frac{1}{2m_R}\frac{\partial^2}{\partial R^2} - \frac{1}{2m_r}\frac{\partial^2}{\partial r^2} + \frac{(\hat{J} - \hat{j})^2}{2m_R R^2} + \frac{\hat{j}^2}{2m_r r^2} + V(R, r, \theta) \quad (1)$$

DOI: 10.1021/acs.jpca.8b06442
J. Phys. Chem. A 2018, 122, 7540−7547

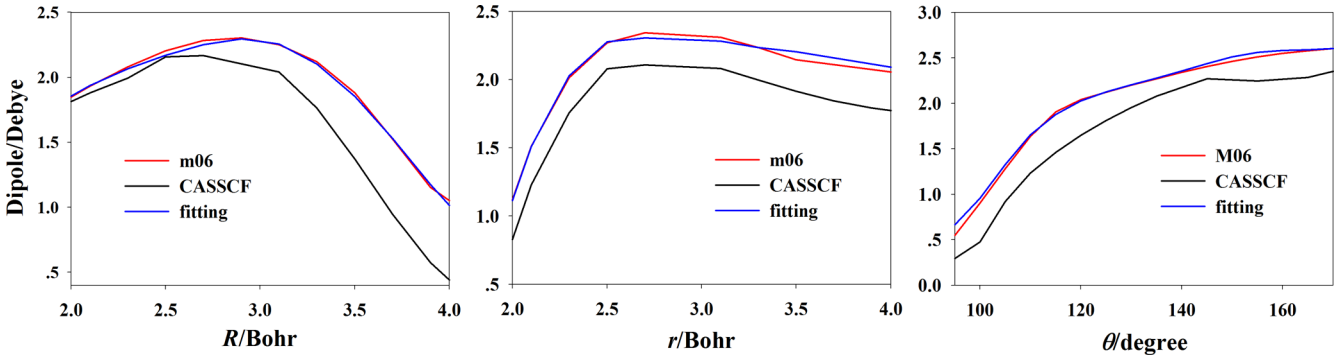

Figure 2. Dipole moment of the HO_2 system along the H + OO Jacobi coordinates R (left), r (middle) and θ (right), while the other coordinates are fixed at R = 3.0 bohr, r = 2.5 bohr, and θ = 134.9°.

where R is the distance from H to the center of mass of the O_2 fragment, r is the O−O internuclear distance, θ is the angle between R and r, $\hat{J}$ and $\hat{j}$ are the total and O−O diatomic angular momentum operator, respectively, and m_R and m_r are the reduced masses of H−O_2 and O_2, respectively. The vibrational states are calculated using the Lanczos algorithm.[26−28] We use 80 ($R \in [0.5,7.0]$ bohr) and 100 ($r \in [1.0,5.5]$ bohr) discrete variable representation (DVR) grids for both R and r.[33] For the angular variable, a 160-point Gauss−Legendre grid is used. The large basis set in our calculation has been tested to ensure the convergence. Since only the vibrational states corresponding to the odd O−O exchange parity are of interest in our case, half of the DVR points in the angle coordinate are discarded in the actual calculations. The converged vibrational energy levels up to approximately 18000 cm^{-1} are generated by carrying out approximately 40,000 Lanczos recursion steps.

The energy levels and wave functions of the bound states of the HO_2 complex are obtained using the iterative Lanczos algorithm. The Lanczos states $|\varphi_k\rangle$are generated from a normalized state of $|\varphi_1\rangle$[28,34]

$$|\varphi_{k+1}\rangle = \beta_k^{-1}[\hat{H}|\varphi_k\rangle - \alpha_k|\varphi_k\rangle - \beta_{k-1}|\varphi_{k-1}\rangle], \; k \geq 1 \tag{2}$$

and

$$\alpha_k = \langle\varphi_k|\hat{H}|\varphi_k\rangle - \langle\varphi_k|\beta_{k-1}|\varphi_{k-1}\rangle \tag{3}$$

$$\beta_k = \langle\hat{H}\varphi_k - \alpha_k\varphi_k - \beta_{k-1}\varphi_{k-1}|\hat{H}\varphi_k - \alpha_k\varphi_k - \beta_{k-1}\varphi_{k-1}\rangle^{1/2} \tag{4}$$

where $\beta_0 = 0$ for the diagonal and sub/superdiagonal elements of the tridiagonal Lanczos matrix. When the total iteration steps are set as N, the corresponding eigenvalues and eigenvectors sets of the Lanczos matrix are $\{E_i^{(N)}\}$and $\{Z_i^{(N)} = [z_{1i}^{(N)},\cdots, z_{Ni}^{(N)}]^T\}$. Then, the wave functions can be expressed by eigenvectors with the basis set of Lanczos states, $|\varphi_k\rangle$, i.e., $|E_i^{(N)}\rangle = \sum_{k=1}^{N} z_{ki}^{(N)}|\varphi_k\rangle$.

The transition dipole moment $\vec{\mu}_{mk}$ can be calculated as $\langle E_m^{(N)}|\vec{u}|E_k^{(N)}\rangle$ with the dipole moment $\vec{u}$. The transition dipole calculated using variational wave functions and dipole surfaces give results that depend on how the Cartesian axes of the dipole surface are defined. Sueur has suggested that the most consistent definition of these axes uses the rules proposed by Eckart for the separation of rovibrational motion.[35] For the triatomic HO_2 system, the Eckart conditions can be easily satisfied by placing the molecule in the body-fixed xz plane. The new set of axes XZ are related to the original axes by a rotation through τ and

$$\tan\tau = \frac{\sum_{i=1}^{3} m_i(x_i^e z_i - z_i^e x_i)}{\sum_{i=1}^{3} m_i(x_i^e x_i + z_i^e z_i)} \tag{5}$$

where the superscript e means the reference coordinate, and i is the atom index.

The dipole moment of HO_2 is computed at the DFT/PVTZ level with the M06 functional. In the region of $R \in [0.5,7.0]$ bohr, $r \in [1.0,5.5]$ bohr, and $\theta \in [0,\pi/2]$ radian at the Jacobi coordinate, 16770 available random Monte Carlo generated points are computed and fitted to the dipole moment surface. The RMSE values of the fits are 0.07 and 0.05 D for the projected components along the x and z directions, respectively, and the relative errors are less than 1% for both directions. A more reliable method, the complete active space self-consistent field (CASSCF) method (10 active orbital and 9 active electrons with cc-PVTZ basis set)[36] is chosen to test the dipole moment values calculated by DFT.

RESULTS AND DISCUSSION

In Figure 2, the fitted DMS is compared with the *ab initio* results in three dimensions of the H + OO Jacobi coordinates. It is clear that the fitting result provides a faithful representation of the DFT result. Compared to the CASSCF results, the DFT calculation overestimates the dipole moment overall but reproduces the trend along the three different directions. In this work, we focus on the general dipole transition behavior between molecular vibrational states, and thus, the behavior should be system independent. Therefore, the DFT method and NN fitting are suitable for the aim of present work, and the use of a more accurate and expansive *ab initio* method is unnecessary.

In Table 1, the calculated energies of the low-lying vibrational states are listed with some reported theoretical and experimental results, where v_1, v_2, and v_3 denote the vibrational quantum numbers for the H−O stretching, O−O stretching and bending modes, respectively. Our values are in good agreement with the previously obtained results, especially the result reported in Xie's work (listed in the "spline" column).[37] In fact, our calculation use the same PES and a slightly different basis set compared to that used in Xie's work. The large basis set in our calculation makes the result reliable according to our tests about the convergence.

DOI: 10.1021/acs.jpca.8b06442
J. Phys. Chem. A 2018, 122, 7540−7547

Table 1. Energies(cm^{-1}) of Low-Lying Vibrational States

(v_1,v_2,v_3)	spline[a]	Xu[b]	Mandelshtam[c]	this work	expt
(0,0,0)	0.00	0.00	0.00	0.00	
(0,0,1)	1090.27	1090.65	1065.46	1089.95	1097.6[d]
(0,1,0)	1387.72	1389.00	1296.37	1388.33	1391.8[d]
(0,0,2)	2162.51	2063.41	2091.15	2161.96	
(0,1,1)	2460.89	2462.47	2359.49	2461.52	
(0,2,0)	2752.26	2752.29	2516.69	2751.23	
(0,0,3)	3215.98	3217.06	3081.04	3215.60	
(1,0,0)	3442.58	3429.99	3333.65	3442.60	3436.2[e]
(0,1,2)	3517.17	3519.24	3386.96	3517.65	
(0,2,1)	3807.07	3808.67	3589.81	3807.16	
(0,3,0)	4090.59	4090.73	3725.79	4088.63	
(0,0,4)	4250.74	4251.63	4041.24	4250.68	
(1,0,1)	4524.51	4514.37	4421.45	4524.26	
(0,1,3)	4558.12	4559.22	4368.54	4558.30	
(1,1,0)	4803.89	4795.11	4688.34	4804.13	
(0,2,2)	4848.98	4850.45	4615.59	4848.46	
(0,3,1)	5128.29	5130.00	4817.06	5126.78	
(0,0,5)	5266.44	5267.13	4975.87	5266.82	
(0,4,0)	5401.39	5404.25	4944.42	5401.07	
(0,1,4)	5567.14	5566.08	5332.53	5567.23	
(1,0,2)	5602.06	5595.27	5447.87	5601.76	
(0,2,3)	5853.92	5850.74	5610.63	5853.81	
(1,1,1)	5885.05	5882.05	5742.99	5884.36	
(1,2,0)	6132.43	6127.15	5911.88	6131.53	
(0,3,2)	6160.61	6158.64	5850.98	6157.71	
(0,0,6)	6262.30	6262.45	5888.57	6263.39	
(0,4,1)	6423.79	6425.61	6052.06	6421.48	
(0,1,5)	6570.53	6571.62	6270.31	6571.08	
(2,0,0)	6646.10	6643.20	6492.28	6645.96	6651.2[f]
(1,0,3)	6670.95	6628.69	6420.90	6671.00	
(0,5,0)	6686.49	6692.89	6155.46	6689.52	
(0,2,4)	6865.39	6866.51	6576.80	6865.33	

[a]Reference 37. [b]Reference 18. [c]Reference 38. [d]Reference 19. [e]Reference 20. [f]Reference 39.

Figure 3 displays the calculated and observed IR spectra for HO_2. There are three main peaks observed at 1089.9 (v_3), 1388.3 (v_2), and 3442.6 (v_1) cm^{-1}, which are in agreement with the experimental spectrum. The relative intensities of the three observed absorption peaks are in excellent agreement with the experimental results.[40] Ignoring the additional absorption peaks of O_3 and H_2O_2, this agreement shows that the XXZLG PES and DMS calculated by DFT are both reliable even though we only used the qualitatively corrected DFT method to calculate the dipole moment.

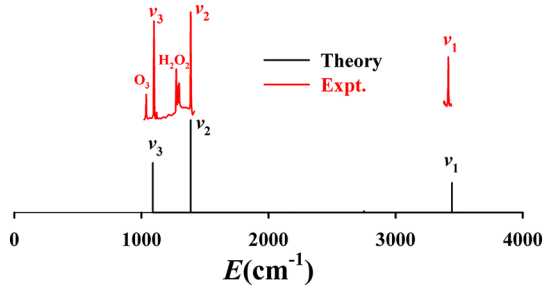

Figure 3. IR absorption spectrum of the vibrational ground state of HO_2.

According to Fermi's golden rule, the vibronic transition moment ($\vec{\mu}_{mk}$) between the different rovibrational states is an important parameter for the external photon field intervention reactions. In Figure 4, the statistical behaviors for the $|\vec{\mu}_{mk}|^2$ values of the HO_2 system are shown by scatter plots. The nonzero vibronic transition moment is close to a band distribution in all of the panels, and the larger transition moment is close to a linear distribution. For much of the data, the vibronic transition moment is larger than 10^{-4}, implying that the HO_2 system can be adjusted using high strength light. The linear distribution for the larger $|\vec{\mu}_{mk}|^2$ is roughly determined by the selection rules of the Raman effect.[41] The rule is that if the dipole moment has a linear or quadratic dependence on the coordinate, the vibronic transition dipole moment vanishes unless the relevant vibrational states are adjacent and both of them belong to the same vibrational mode.

Figure 4 shows an interesting case where the linear distribution of the large transition moment is destroyed for the high energy states. This must arise from the anharmonic and coupling effects between the different vibrational modes. Considering that the energy of the microwave radiation is very small, this feature must be useful for the microwave-involved reactions. When Fermi's golden rule of $2\pi | \vec{\mu}_{mk}\cdot\vec{E} |^2 \delta(\omega_{mk} - \omega)/h^2$ is used to consider the stimulated absorption and the emission of the photons in addition to the transition moment $\vec{\mu}_{mk}$, the resonance part, which is described by the delta function, is also very important. We can use different frequencies of the photon to affect different reactions. For the HO_2 system, many $\vec{\mu}_{mk}$ are nonzero, implying that we can use different photon frequencies to control this reaction. Obviously, this conclusion can be extended to other reactions.

The high-energy vibrational states in our calculations approach the reactive energy of the H + O_2 ↔ O + OH reaction, and these states have the larger transition moment relative to their adjacent states (difference of a few wavenumbers), as shown in Figure 4. We also know that the energy of microwave irradiation is in the 0.01−10.0 cm^{-1} range. Therefore, in principle, microwave irradiation can be used to affect the H + O_2 ↔ O + OH reactions. Because of the rather large dipole moment of HO_2, the transition between the adjacent rotational states driven by microwave irradiation must occur very easily. However, the transition behavior of the rotational states is not the focal point of this work.

The bottom left panel of Figure 4 shows that the distribution of the larger transition moments is located along few lines. This means that in the absence of collision relaxation events, the high-energy states can release their energies to the vibrational ground state step by step through spontaneous transitions. This feature must be very useful in time-resolved vibrational spectroscopy.[42−45] In Figure 5, the scatter plot of the statistical behavior for the $\omega_{mk}{}^3|\vec{\mu}_{mk}|^2$ (the factor of $\omega_{mk}{}^3$comes from the difference between the spontaneous transition and the stimulated radiation, and ω_{mk} is the energy difference between the m and k states) values of the HO_2 system and the two possible energy release paths of the predissociation states of X^3 and X^4 are presented. The asymptotes of H + O_2 are marked by the purple star symbol on the axis. The purple arrows I−IV mark the four main emission bands in the energy range of 1300−7000 cm^{-1}, and the energy range agrees with the experimental results reported by Polanyi.[45] Two possible energy release paths are shown by

DOI: 10.1021/acs.jpca.8b06442
J. Phys. Chem. A 2018, 122, 7540−7547

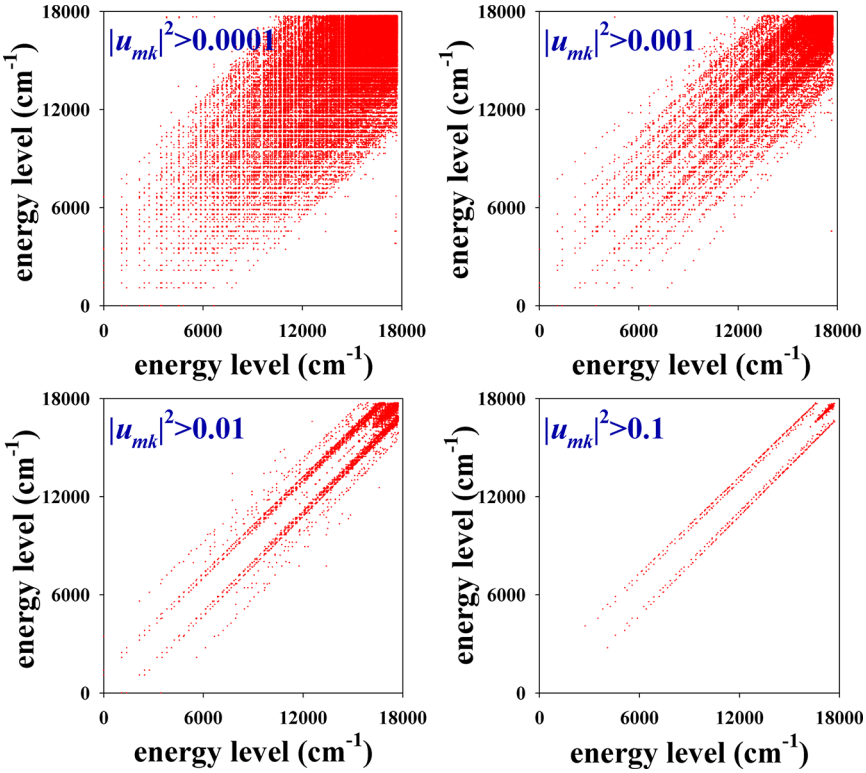

Figure 4. Scatter plot of the statistical behavior for $|\vec{\mu}_{mk}|^2$ values of the HO_2 system ($J = 0$), where the vibrational states are presented according to their energy levels to replace the m and k subscripts.

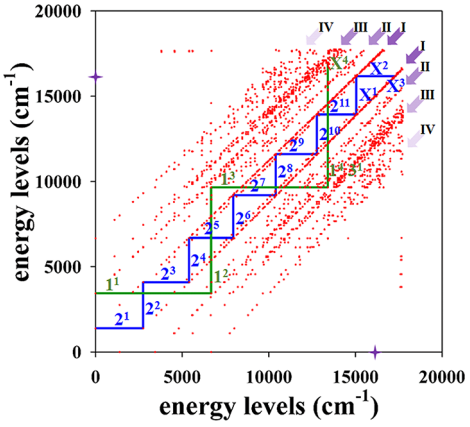

Figure 5. Scatter plot of the statistical behavior for the $\omega_{mk}{}^3|\vec{\mu}_{mk}|^2$ values of the HO_2 system and two possible energy-release paths of a predissociation state. The asymptotes of H + O_2 are marked by the purple star symbol on the axis. The purple arrows I–IV mark the four main emission bands at approximately 1400, 2600, 3800, and 5500 cm^{-1}. Two possible energy-release paths are shown by blue and green lines with the assignments of the corresponding states. Labels 2^1 to 2^{11} indicate the pure O–O vibrational excitation states, labels 1^1 to 1^3 indicate the pure O–H vibrational excitation, X^1–X^3 are the mixed states involving O–O vibrational excitation mainly, and X^4 is a mixed state involving O–H vibrational excitation.

the blue and green lines with the assignments of the corresponding states. The labels 2^1 to 2^{11} indicate the pure O–O vibrational excitation states, the labels 1^1 to 1^3 indicate the pure O–H vibrational excitation, X^1-X^3 are the mixed states mainly involving the O–O vibrational excitation, and X^4 is a mixed state involving the O–H vibrational excitation. In other words, the high-energy HO_2 radical generated in the H + O_2 ↔ O + OH reactions can release its energy via step by step photon emission, coinciding with the luminescence process in the combustion. We can see that the possible paths of the high-energy vibration energy release are abundant, which is not discussed in detail in this work. Examination of Figure 5 clearly shows that spontaneous emission in the microwave range is very unlikely due to the small Einstein coefficient increasing the small energy difference. This means that microwave light will be very effective in contributing energy into the system, which is the one of the intrinsic mechanisms of microwave heating.

In the present work, we focus on the calculation of the vibronic transition moment for the HO_2 radical. The transition moment between the rotational states is also important for the microwave-induced reactions. We know that the dipole moment of the HO_2 complex is large enough to induce rotational excitation. The rotational spectroscopy of the HO_2 system had been studied by many experimental techniques.[19,20,46] At a high-resolution level, dozens of rotational absorption peaks can be observed in all of the ν_1, ν_2 and ν_3 fundamental absorption bands. This feature of the rotational quantum states is also beneficial for microwave processes.

In Figure 6, the wave functions of the six high-energy vibrational states of HO_2 are shown in the r–R plane, while the transition dipole moments between all of the calculated states and these six states are plotted in Figure 7. The state at 10,980 cm^{-1} is an excited one along the R direction, the states at 14 603, 16 400 and 17 473 cm^{-1} are mainly due to O–O excitations, while the states at 15 222 and 17 306 cm^{-1} are due to mixed excitations. We can see a few main peaks, and many of the visible peaks in the corresponding transition dipole moment plots are shown in Figure 7. If the approach of

DOI: 10.1021/acs.jpca.8b06442
J. Phys. Chem. A 2018, 122, 7540–7547

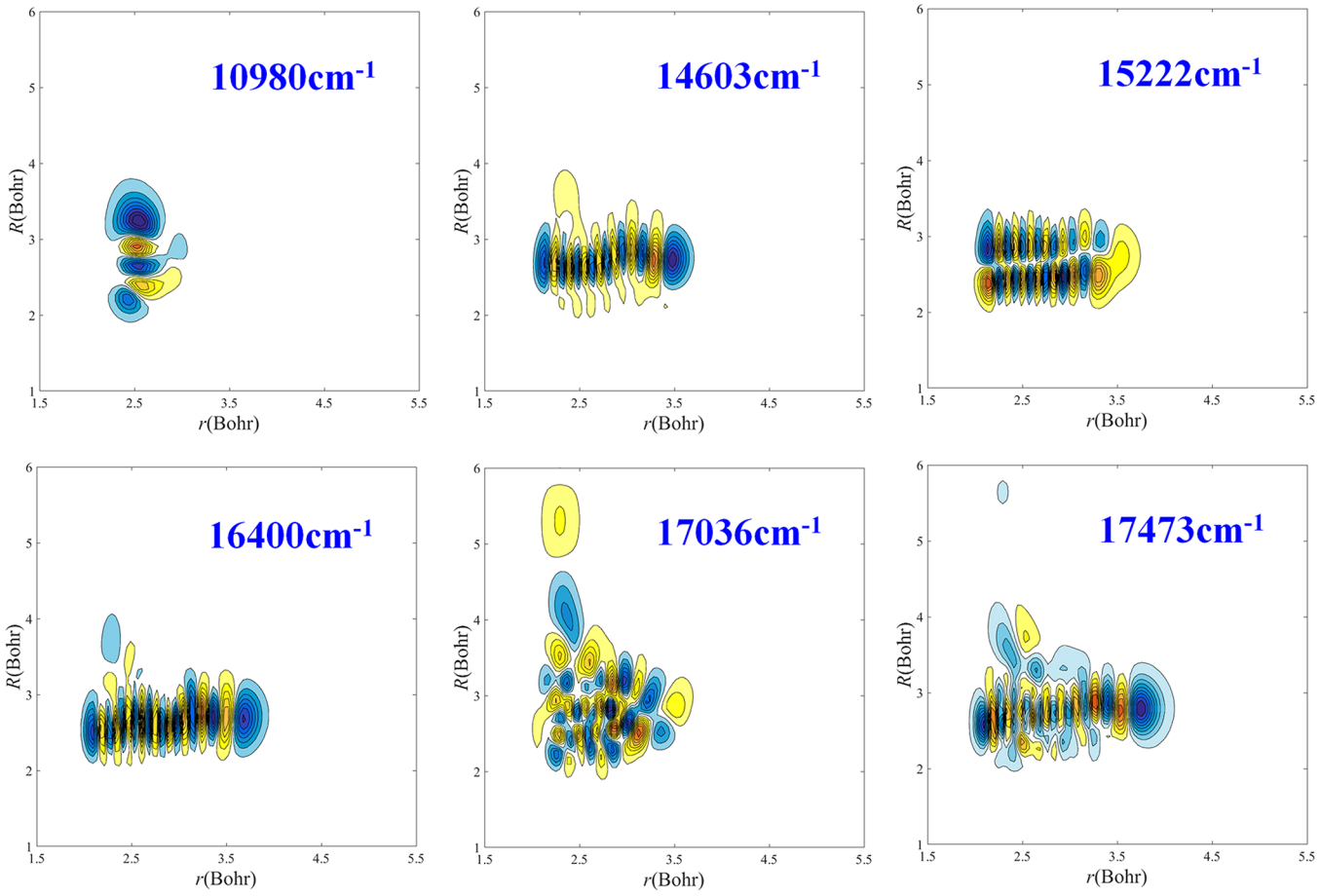

Figure 6. Wave functions of the six vibrational states of HO_2.

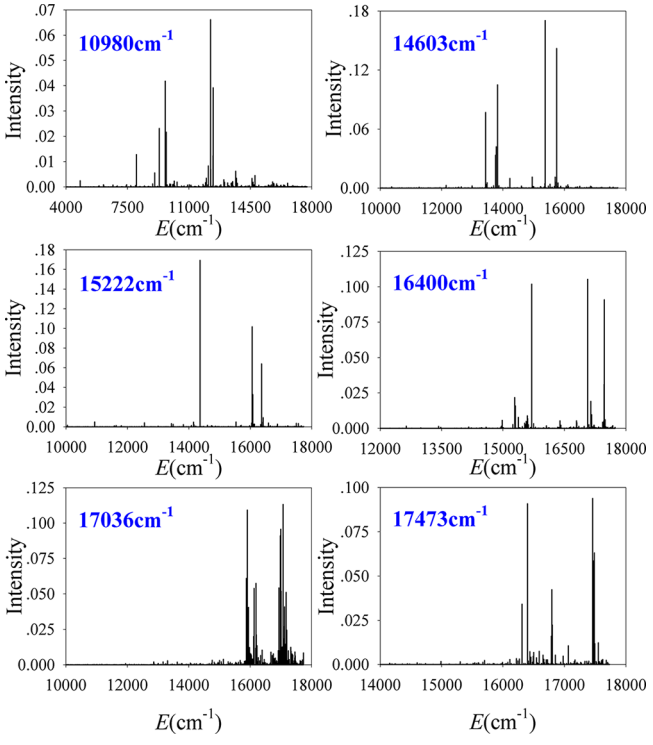

Figure 7. IR absorption spectrum of the six vibrational states shown in Figure 6.

photodynamics is to be used to intervene or control the H + O_2 ↔ O + OH reactions, it must be frequency sensitive.

In Table 2, we list the energy differences and changes in the vibrational modes for three of the adjacent states that have larger transition dipole moments relative to each state shown in Figure 6. For the state at 10,980 cm^{-1}, there are three peaks located at +35.7, −55.6, and −818.7 cm^{-1} relative to the 10 980 cm^{-1} state, and these energy differences are in the infrared and far-infrared regions of the light spectrum. We can see that the vibrational modes have obvious changes for all of the three states. For example, the ν_1, ν_2 and ν_3 vibrational modes change −2, 1, and 6 energy levels, respectively, even though the energy difference is only 35.7 cm^{-1}. For the higher energy states of 17 473 cm^{-1}, the three peaks are located at −3.6, +12.1, and +21.7 cm^{-1} relative to 17 473 cm^{-1} with energy differences in the microwave region. Here, as well, the vibrational modes change significantly for all of the states. This means that the mode-specific and bond-selective reactions should be affected by microwave irradiation in the complex region.

CONCLUSIONS

In summary, a procedure for the activation of chemical reactions in the complex region is proposed and discussed for a model H + O_2 ↔ O + OH reaction system. Two important factors for the effective control of the reaction by microwave irradiation are investigated. The factors are (1) whether the transition dipole moment between the adjacent quantum states within the range of the microwave energy is large enough and

DOI: 10.1021/acs.jpca.8b06442
J. Phys. Chem. A 2018, 122, 7540−7547

Table 2. Energy Differences (in cm^{-1}) and Changes in the Vibrational Modes for Three of the Adjacent States That Have a Larger Transition Dipole Moment Relative to Each State Shown in Figure 6[a]

energy levels	ΔE	$\Delta\nu_1\Delta\nu_2\Delta\nu_3$	ΔE	$\Delta\nu_1\Delta\nu_2\Delta\nu_3$	ΔE	$\Delta\nu_1\Delta\nu_2\Delta\nu_3$
10 980	35.7	$1^{-2}2^{1}3^{6}$	−55.6	$1^{-3}2^{6}3^{4}$	−818.7	$1^{-3}2^{6}3^{3}$
14 603	−4.6	$1^{2}2^{7}3^{-7}$	10.2	$1^{1}2^{7}3^{-12}$	62.0	$1^{2}2^{3}3^{-11}$
15 222	−34.2	$1^{1}2^{2}3^{-7}$	62.4	$1^{0}2^{2}3^{-3}$	−81.4	$1^{-1}2^{5}3^{-2}$
16 400	−8.8	$1^{5}2^{1}3^{-16}$	17.2	$1^{1}2^{3}3^{-7}$	12.7	$1^{1}2^{7}3^{-11}$
17 036	8.9	$1^{-1}2^{3}3^{0}$	−37.4	$1^{1}2^{1}3^{-3}$	−24.4	$1^{-1}2^{1}3^{-3}$
17 473	−3.6	$1^{-1}2^{2}3^{-2}$	12.1	$1^{2}2^{2}3^{-11}$	21.7	$1^{2}2^{-1}3^{-5}$

[a]The change of each vibrational mode is denoted by the corresponding superscript. For example, $\Delta\nu_1\Delta\nu_2\Delta\nu_3 = 1^{1}2^{7}3^{-12}$ represents the fact that the ν_1 and ν_2 modes are excited by 1 and 7 levels, respectively, and the ν_3 mode relaxes by 12 levels.

(2) whether the vibrational mode of the transition allowed adjacent states to change obviously. For the H + O_2 ↔ O + OH triatomic reaction, the answers to both questions are positive. In general, a system that has more atoms and a larger polarity is more likely to meet these two conditions. Without a loss of generality, the triatomic H + O_2 ↔ O + OH reaction is used to check for these two conditions numerically. The existence of a nonzero transition dipole moment between the two nearly degenerate vibrational states allows us to use microwave irradiation to affect complex reactions.

Furthermore, in our previous work, we proposed a theoretical description for both thermal effects and nonthermal microwave effects using the state-specific master equation approach.[47] Microwave enhancement of reactivity arises from two important mechanisms. (1) The microwave absorption and emission dominated by the transition dipole moment between two corresponding states and the intensity of the microwave field may provide a new path to change the reaction rate constants. (2) In a strong microwave field, the distribution of the activated internal states of the molecules will deviate from the equilibrium distribution. The transition dipole moment plays a key role for both of the mechanisms. The existence of a nonzero transition dipole moment between two nearly degenerate vibrational states strongly supports our master equation results. And in our previous work,[47] the mechanism of the microwave effect in chemical reactions had been discussed in detail.

A detailed analysis based on the vibrational structures of the corresponding wave functions shows that the change of the vibrational modes is obvious even when the energy difference between the two transition allowed states is very small (in few wavenumbers). This phenomenon shows that inexpensive and powerful microwave irradiation can be used to affect and possibly control mode-specific and bond-selective reactions. Our calculations also show that the predissociation state of the H + O_2 ↔ O + OH reactions can release its energy by step by step photon emission, which is a possible luminescence process in combustion.

The H + O_2 ↔ O + OH reaction plays an important role in the combustion processes. The reaction contains a relatively stable complex, and its reaction time is enough long to interact with microwave. The conclusions of this paper also can be applicable to other reactions involving complexes or long lifetimes, such as the OH + CO ↔ H + CO_2 and F + H_2O ↔ HF + OH reactions.[48,49] As mentioned in ref 15, microwaves have a more effective acceleration for the slower reactions. Taking into account that the polyatomic molecules have a large vibrational state density and more stable structures, the above conclusions should be more important for polyatomic molecular reactions. Although this work focuses on the feasibility of using microwave irradiation to affect the mode-specific reactions, the conclusions in this paper are not limited to these reactions only.

AUTHOR INFORMATION

Corresponding Authors

*(J. Ma) E-mail: majianyi81@163.com.
*(S.L.) E-mail: slin@fzu.edu.cn.

ORCID

Dandan Ma: 0000-0002-6146-2001
Sen Lin: 0000-0002-2288-5415

Author Contributions

#These authors contributed equally to this work.

Notes

The authors declare no competing financial interest.

ACKNOWLEDGMENTS

J. Ma and S.L. acknowledge support from the National Natural Science Foundation of China (91441107, 21303110 and 21673040). We also thank Prof. Hua Guo, Bin Jiang and Jun Li for many useful discussions.

REFERENCES

(1) Schranz, H. W.; Raff, L. M.; Thompson, D. L. Intramolecular energy transfer and mode-specific effects in unimolecular reactions of disilane. *J. Chem. Phys.* **1991**, *95*, 106−120.
(2) Sinha, A.; Hsiao, M. C.; Crim, F. F. Controlling bimolecular reactions: Mode and bond selected reaction of water with hydrogen atoms. *J. Chem. Phys.* **1991**, *94*, 4928−4935.
(3) Beck, R. D.; Maroni, P.; Papageorgopoulos, D. C.; Dang, T. T.; Schmid, M. P.; Rizzo, T. R. Vibrational mode-specific reaction of methane on a nickel surface. *Science* **2003**, *302*, 98−100.
(4) Zare, R. N. Laser control of chemical reactions. *Science* **1998**, *279*, 1875−1879.
(5) Chang, X. Y.; Sewell, T. D.; Raff, L. M.; Thompson, D. L. Power spectra as a diagnostic tool in probing statistical/nonstatistical behavior in unimolecular reactions. *J. Chem. Phys.* **1992**, *97*, 7354−7361.
(6) Polanyi, J. C.; Wong, W. H. Location of energy barriers. I. Effect on the dynamics of reactions A + BC. *J. Chem. Phys.* **1969**, *51*, 1439−1450.
(7) Polanyi, J. C. Energy distribution among reagents and products of atomic reactions. *J. Chem. Phys.* **1959**, *31*, 1338−1351.
(8) Jiang, B.; Guo, H. Relative efficacy of vibrational vs. Translational excitation in promoting atom-diatom reactivity: Rigorous examination of polanyi's rules and proposition of sudden vector projection (SVP) model. *J. Chem. Phys.* **2013**, *138*, 234104.
(9) Strazisar, B. R.; Lin, C.; Floyd Davis, H. Mode-specific energy disposal in the four-atom reaction OH + D_2 → HOD + D. *Science* **2000**, *290*, 958−961.

DOI: 10.1021/acs.jpca.8b06442
J. Phys. Chem. A 2018, 122, 7540−7547

(10) Liu, R.; Wang, F.; Jiang, B.; Czakó, G.; Yang, M.; Liu, K.; Guo, H. Rotational mode specificity in the Cl + CHD_3 → HCl + CD_3 reaction. *J. Chem. Phys.* **2014**, *141*, 074310.
(11) Wang, F.; Lin, J.-S.; Liu, K. Steric control of the reaction of CH stretch−excited CHD_3 with chlorine atom. *Science* **2011**, *331*, 900−903.
(12) Wang, Y.; Song, H.; Szabó, I.; Czakó, G.; Guo, H.; Yang, M. Mode-specific SN2 reaction dynamics. *J. Phys. Chem. Lett.* **2016**, *7*, 3322−3327.
(13) Gedye, R.; Smith, F.; Westaway, K.; Ali, H.; Baldisera, L.; Laberge, L.; Rousell, J. The use of microwave ovens for rapid organic synthesis. *Tetrahedron Lett.* **1986**, *27*, 279−282.
(14) de la Hoz, A.; Diaz-Ortiz, A.; Moreno, A. Microwaves in organic synthesis. Thermal and non-thermal microwave effects. *Chem. Soc. Rev.* **2005**, *34*, 164−178.
(15) Kappe, C. O. Controlled microwave heating in modern organic synthesis. *Angew. Chem., Int. Ed.* **2004**, *43*, 6250−6284.
(16) Kaiser, N.-F. K.; Bremberg, U.; Larhed, M.; Moberg, C.; Hallberg, A. Fast, convenient, and efficient molybdenum-catalyzed asymmetric allylic alkylation under noninert conditions: An example of microwave-promoted fast chemistry. *Angew. Chem., Int. Ed.* **2000**, *39*, 3595−3598.
(17) Nuchter, M.; Ondruschka, B.; Bonrath, W.; Gum, A. Microwave assisted synthesis - a critical technology overview. *Green Chem.* **2004**, *6*, 128−141.
(18) Xu, C.; Xie, D.; Zhang, D. H.; Lin, S. Y.; Guo, H. A new ab initio potential-energy surface of $HO_2(X_2A'')$ and quantum studies of HO_2 vibrational spectrum and rate constants for the H + O_2 ↔ O + OH reactions. *J. Chem. Phys.* **2005**, *122*, 244305.
(19) Yamada, C.; Endo, Y.; Hirota, E. Difference frequency laser spectroscopy of the ν_1 band of the HO_2 radical. *J. Chem. Phys.* **1983**, *78*, 4379−4384.
(20) Burkholder, J. B.; Hammer, P. D.; Howard, C. J.; Towle, J. P.; Brown, J. M. Fourier transform spectroscopy of the ν_2 and ν_3 bands of HO_2. *J. Mol. Spectrosc.* **1992**, *151*, 493−512.
(21) Chapman, D.; Bowman, J. M.; Gazdy, B. Time dependence of oh overtone relaxation in the hydroperoxyl radical. *J. Chem. Phys.* **1992**, *96*, 1919−1930.
(22) Blank, T. B.; Brown, S. D.; Calhoun, A. W.; Doren, D. J. Neural network models of potential energy surfaces. *J. Chem. Phys.* **1995**, *103*, 4129−4137.
(23) Brown, D. F. R.; Gibbs, M. N.; Clary, D. C. Combining ab initio computations, neural networks, and diffusion monte carlo: An efficient method to treat weakly bound molecules. *J. Chem. Phys.* **1996**, *105*, 7597−7604.
(24) Behler, J. Neural network potential-energy surfaces in chemistry: A tool for large-scale simulations. *Phys. Chem. Chem. Phys.* **2011**, *13*, 17930−17955.
(25) Raff, L.; Komanduri, R.; Hagan, M.; Bukkapatnam, S. *Neural Networks in Chemical Reaction Dynamics*; Oxford University Press, Inc.: 2012.
(26) Xu, D.; Chen, R.; Guo, H. Probing highly excited vibrational eigenfunctions using a modified single lanczos propagation method: Application to acetylene (HCCH). *J. Chem. Phys.* **2003**, *118*, 7273.
(27) Chen, R.; Guo, H. A single lanczos propagation method for calculating transition amplitudes. II. Modified QL and symmetry adaptation. *J. Chem. Phys.* **2001**, *114*, 1467−1472.
(28) Lanczos, C. An iteration method for the solution of the eigenvalue problem of linear differential and integral operators. *J. Res. Natl. Bur. Stand.* **1950**, *45*, 255−282.
(29) Zhao, Y.; Truhlar, D. G. The M06 suite of density functionals for main group thermochemistry, thermochemical kinetics, noncovalent interactions, excited states, and transition elements: Two new functionals and systematic testing of four M06-class functionals and 12 other functionals. *Theor. Chem. Acc.* **2008**, *120*, 215−241.
(30) Frisch, M. J.; Trucks, G. W.; Schlegel, H. B.; Scuseria, G. E.; Robb, M. A.; Cheeseman, J. R.; Scalmani, G.; Barone, V.; Petersson, G. A.; Nakatsuji, H., et al. *Gaussian 09*, Revision A.01; Gaussian, Inc.: Wallingford, CT, 2009.
(31) Jiang, B.; Guo, H. Permutation invariant polynomial neural network approach to fitting potential energy surfaces. *J. Chem. Phys.* **2013**, *139*, 054112.
(32) Li, J.; Carter, S.; Bowman, J. M.; Dawes, R.; Xie, D.; Guo, H. High-level, first-principles, full-dimensional quantum calculation of the ro-vibrational spectrum of the simplest criegee intermediate (CH_2OO). *J. Phys. Chem. Lett.* **2014**, *5*, 2364−2369.
(33) Light, J. C.; Carrington, T., Jr. Discrete-variable representations and their utilization. *Adv. Chem. Phys.* **2007**, *114*, 263−310.
(34) Ma, J.; Xu, D.; Guo, H.; Tyng, V.; Kellman, M. E. Isotope effect in normal-to-local transition of acetylene bending modes. *J. Chem. Phys.* **2012**, *136*, 014304.
(35) Le Sueur, C. R.; Miller, S.; Tennyson, J.; Sutcliffe, B. T. On the use of variational wavefunctions in calculating vibrational band intensities. *Mol. Phys.* **1992**, *76*, 1147−1156.
(36) Werner, H. J.; Knowles, P. J. A second order multiconfiguration SCF procedure with optimum convergence. *J. Chem. Phys.* **1985**, *82*, 5053−5063.
(37) Xie, D.; Xu, C.; Ho, T.-S.; Rabitz, H.; Lendvay, G.; Lin, S. Y.; Guo, H. Global analytical potential energy surfaces for $HO_2(X^2A'')$ based on high level ab initio calculations. *J. Chem. Phys.* **2007**, *126*, 074315.
(38) Mandelshtam, V. A.; Grozdanov, T. P.; Taylor, H. S. Bound states and resonances of the hydroperoxyl radical HO_2. An accurate quantum mechanical calculation using filter diagonalization. *J. Chem. Phys.* **1995**, *103*, 10074.
(39) DeSain, J. D.; Ho, A. D.; Taatjes, C. A. High-resolution diode laser absorption spectroscopy of the O-H stretch overtone band (2,0,0)←(0,0,0) of the HO_2 radical. *J. Mol. Spectrosc.* **2003**, *219*, 163−169.
(40) Smith, D. W.; Andrews, L. Argon matrix infrared spectra and vibrational analysis of the hydroperoxyl and deuteroperoxyl free radicals. *J. Chem. Phys.* **1974**, *60*, 81−85.
(41) Albrecht, A. C. On the theory of raman intensities. *J. Chem. Phys.* **1961**, *34*, 1476−1484.
(42) Milligan, D. E.; Jacox, M. E. Infrared spectroscopic evidence for the species HO_2. *J. Chem. Phys.* **1963**, *38*, 2627−2631.
(43) Sagnella, D. E.; Straub, J. E.; Jackson, T. A.; Lim, M.; Anfinrud, P. A. Vibrational population relaxation of carbon monoxide in the heme pocket of photolyzed carbonmonoxy myoglobin: Comparison of time-resolved mid-IR absorbance experiments and molecular dynamics simulations. *Proc. Natl. Acad. Sci. U. S. A.* **1999**, *96*, 14324.
(44) Walther, M.; Fischer, B.; Schall, M.; Helm, H.; Jepsen, P. U. Far-infrared vibrational spectra of all-trans, 9-cis and 13-cis retinal measured by THz time-domain spectroscopy. *Chem. Phys. Lett.* **2000**, *332*, 389−395.
(45) Charters, P. E.; Polanyi, J. C. An improved technique for the observation of infrared chemiluminescence: Resolved infrared emission of OH arising from the system H + O_2. *Can. J. Chem.* **1960**, *38*, 1742−1755.
(46) McKellar, A. R. W. Laser magnetic resonance spectroscopy of the ν_2 fundamental band of DO_2 at 9.8 μm. *J. Chem. Phys.* **1979**, *71*, 81−88.
(47) Ma, J. Master equation analysis of thermal and nonthermal microwsave effects. *J. Phys. Chem. A* **2016**, *120*, 7989−7997.
(48) Ma, J.; Li, J.; Guo, H. Quantum dynamics of the HO + CO → H + CO_2 reaction on an accurate potential energy surface. *J. Phys. Chem. Lett.* **2012**, *3*, 2482−2486.
(49) Otto, R.; Ma, J.; Ray, A. W.; Daluz, J. S.; Li, J.; Guo, H.; Continetti, R. E. Imaging dynamics on the F + H_2O → HF + OH potential energy surfaces from wells to barriers. *Science* **2014**, *343*, 396−399.

DOI: 10.1021/acs.jpca.8b06442
J. Phys. Chem. A 2018, 122, 7540−7547